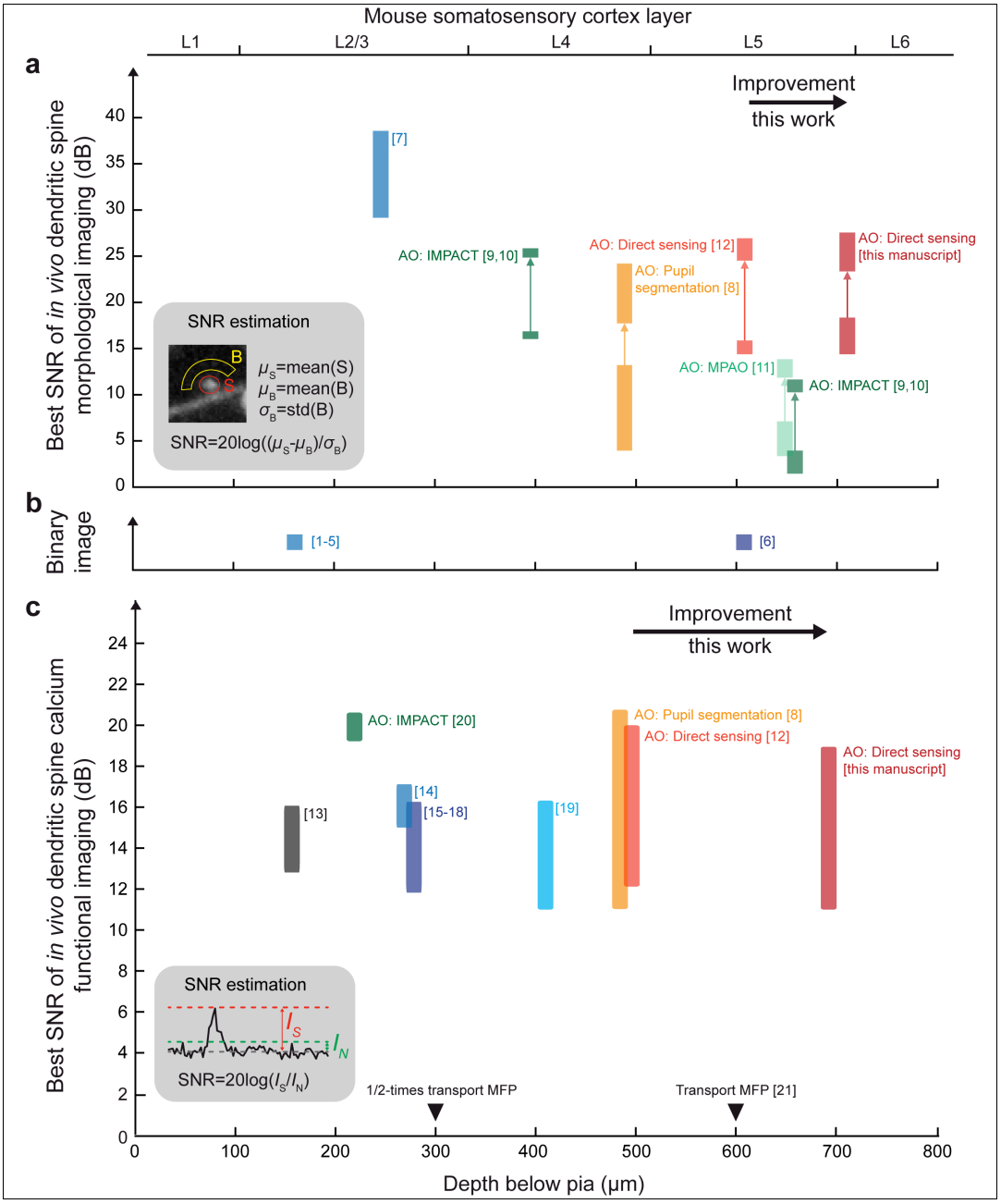
Mouse somatosensory cortex layer
L1
L2/3
L4
L5
L6
a
Improvement
this work
Best SNR of in vivo dendritic spine morphological imaging (dB)
[7]
AO: IMPACT [9,10]
AO: Direct sensing [12]
AO: Pupil segmentation [8]
AO: Direct sensing [this manuscript]
AO: MPAO [11]
AO: IMPACT [9,10]
SNR estimation
B
S
μS=mean(S)
μB=mean(B)
σB=std(B)
SNR=20log((μS-μB)/σB)
b
Binary image
[1-5]
[6]
c
Improvement
this work
Best SNR of in vivo dendritic spine calcium functional imaging (dB)
AO: IMPACT [20]
[13]
[14]
[15-18]
[19]
AO: Pupil segmentation [8]
AO: Direct sensing [12]
AO: Direct sensing [this manuscript]
SNR estimation
IS
IN
SNR=20log(IS/IN)
1/2-times transport MFP
Transport MFP [21]
Depth below pia (μm)

Supplementary Figure 1

The best signal-to-noise ratio (SNR) of *in vivo* dendritic spine morphological and calcium imaging in previous published work

(a, b) Comparison of *in vivo* dendritic spine morphological imaging SNR among previous works using traditional two-photon microscopy or with adaptive optics at different depth. Subgraph in the bottom left corner of **a** shows how to estimate SNR. The images for SNR estimation are directly imported from the publications. The arrows in panel **a** indicate the increase of the SNR by adaptive optics.

Microsoft Office User 4/23/2019 7:28 PM
Deleted: the

(c) Comparison of *in vivo* dendritic spine calcium functional imaging SNR among previous works using traditional two-photon microscopy or with adaptive optics at different depth. Subgraph in the bottom left corner shows how to the estimate the SNR of dendritic spine calcium signal.

References noted in figure panels:

1 Yang, G., Pan, F. & Gan, W. B. Stably maintained dendritic spines are associated with lifelong memories. *Nature* **462**, 920-924 (2009).

2 Grutzendler, J., Kasthuri, N. & Gan, W. B. Long-term dendritic spine stability in the adult cortex. *Nature* **420**, 812-816 (2002).

3 Xu, T. H. *et al.* Rapid formation and selective stabilization of synapses for enduring motor memories. *Nature* **462**, 915-919 (2009).

4 Holtmaat, A., Wilbrecht, L., Knott, G. W., Welker, E. & Svoboda, K. Experience-dependent and cell-type-specific spine growth in the neocortex. *Nature* **441**, 979-983 (2006).

5 Trachtenberg, J. T. *et al.* Long-term *in vivo* imaging of experience-dependent synaptic plasticity in adult cortex. *Nature* **420**, 788-794 (2002).

6 Holtmaat, A. *et al.* Long-term, high-resolution imaging in the mouse neocortex through a chronic cranial window. *Nat Protoc* **4**, 1128-1144 (2009).

7 Chen, J. L. *et al.* Clustered dynamics of inhibitory synapses and dendritic spines in the adult neocortex. *Neuron* **74**, 361-373 (2012).

8 Wang, C. *et al.* Multiplexed aberration measurement for deep tissue imaging *in vivo*. *Nature Methods* **11**, 1037-1040 (2014).

9 Kong, L. J. & Cui, M. *In vivo* deep tissue imaging via iterative multiphoton adaptive compensation technique. *IEEE J Select Topic Quant Elect* **22** (2016).

10 Kong, L. J. & Cui, M. *In vivo* neuroimaging through the highly scattering tissue via iterative multi-photon adaptive compensation technique. *Optics Express* **23**, 6145-6150 (2015).

11 Park, J. H., Kong, L. J., Zhou, Y. F. & Cui, M. Large-field-of-view imaging by multi-pupil adaptive optics. *Nature Methods* **14**, 581-583 (2017).

12 Wang, K. *et al.* Direct wavefront sensing for high-resolution *in vivo* imaging in scattering tissue. *Nature Communications* **6**, 7276 (2015).

13 Chen, T. W. *et al.* Ultrasensitive fluorescent proteins for imaging neuronal activity. *Nature* **499**, 295-300 (2013).

14 Kerlin, A. *et al.* Functional clustering of dendritic activity during decision-making. *BioRxiv*, (2018).

15 Jia, H. B., Rochefort, N. L., Chen, X. W. & Konnerth, A. Dendritic organization of sensory input to cortical neurons *in vivo*. *Nature* **464**, 1307-1312 (2010).

16 Varga, Z., Jia, H. B., Sakmann, B. & Konnerth, A. Dendritic coding of multiple sensory inputs in single cortical neurons *in vivo*. *Proc Natl Acad Sci USA* **108**, 15420-15425 (2011).

17 Jia, H. B., Rochefort, N. L., Chen, X. W. & Konnerth, A. *In vivo* two-photon imaging of sensory-evoked dendritic calcium signals in cortical neurons. *Nat Protoc* **6**, 28-35 (2011).

18 Chen, X. W., Leischner, U., Rochefort, N. L., Nelken, I. & Konnerth, A. Functional mapping of single spines in cortical neurons *in vivo*. *Nature* **475**, 501-505 (2011).

19 Jia, H. B., Varga, Z., Sakmann, B. & Konnerth, A. Linear integration of spine Ca^{2+} signals in layer 4 cortical neurons *in vivo*. *Proc Natl Acad Sci USA* **111**, 9277-9282 (2014).

20 Kong, L. & Cui, M. *In vivo* fluorescence microscopy via iterative multi-photon adaptive compensation technique. *Optics Express* **22**, 23786-23794 (2014).

21 Ntziachristos, V. Going deeper than microscopy: the optical imaging frontier in biology. *Nature Methods* **7**, 603-614 (2010).

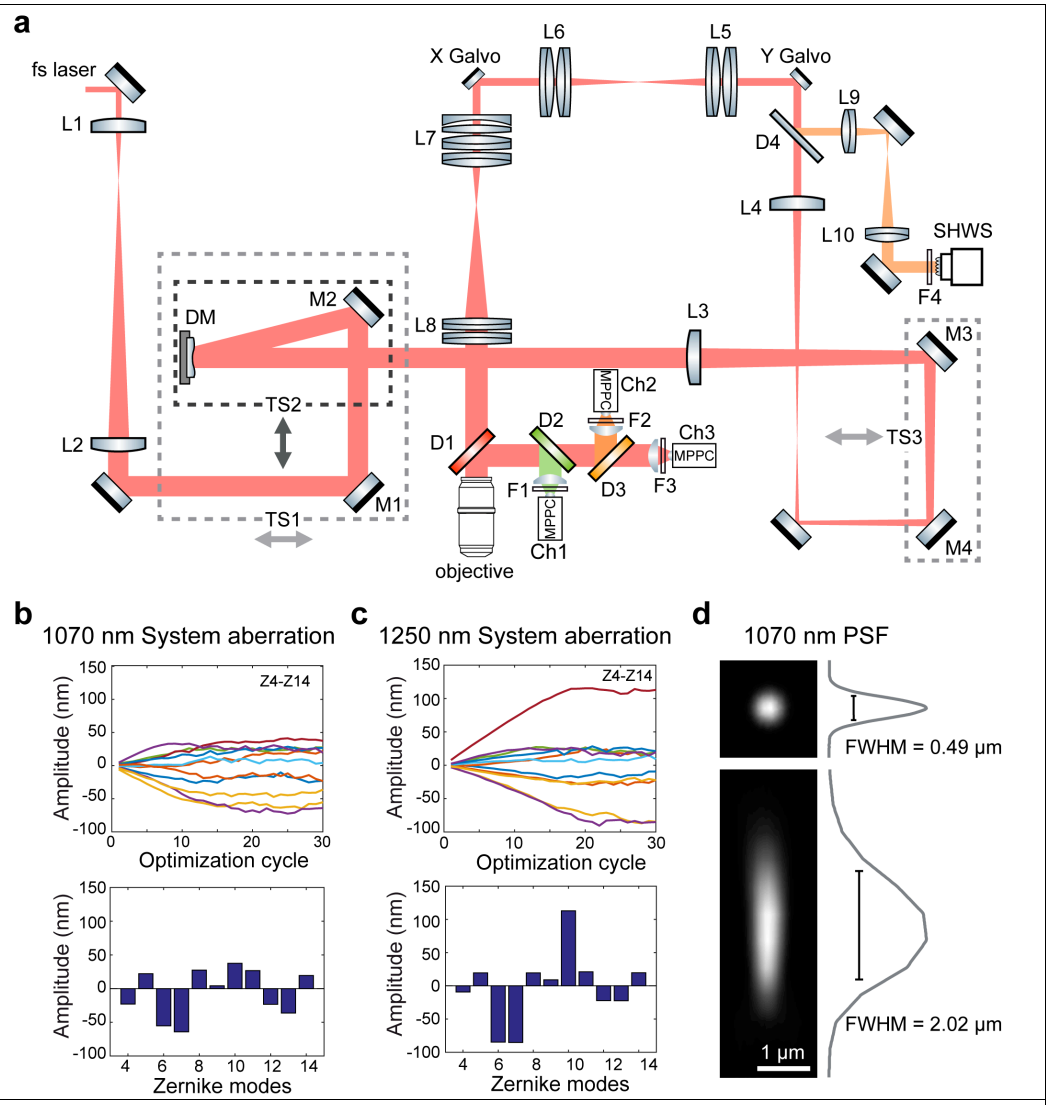

Supplementary Figure 2

Schematic and calibration of direct wavefront sensing two-photon microscope setup

(a) A tunable femtosecond beam is expanded and incident on the deformable mirror (DM). The DM,

the X and Y galvo mirrors, and the back focal plane of the objective are all conjugated by the 4-f lens pair between each other. The Shack-Hartmann wavefront sensor (SHWS) is placed in a descan mode. The microlens array of the SHWS is further conjugated with the objective back focal place. During wavefront sensing, the fluorescence emission light is descanned and separated with the guide star excitation beam by dichroic D4 before arriving at the microlens array of the SHWS. Function signals are collected onto multi-pixel photon counters.

(b,c) System AO aberration calibration. Top panels show the changes of Zernike mode coefficients as a function of optimization cycles. Bottom panels show the system aberration represented by Zernike mode index at wavelengths of 1.07 μm and 1.25 μm after 30 cycles optimization.

(d) Lateral and axial images and signal profiles of a 200-nm diameter fluorescent bead imaged at 1070-nm wavelength.

Microsoft Office User 4/23/2019 7:32 PM
Comment [1]: "... Zernike modes change..." or "...Zernike mode changes..."? Also. Is it correct that there are two "changes" in this sentence? In other words, I don't think I understand this sentence. It might be worth rephrasing.

Rui Liu 4/26/2019 4:26 PM
Comment [2R1]: corrected

Rui Liu 4/26/2019 4:23 PM
Deleted: amplitude of

Rui Liu 4/26/2019 4:23 PM
Deleted: s

Rui Liu 4/26/2019 4:23 PM
Deleted: changes

Rui Liu 4/26/2019 4:23 PM
Deleted:

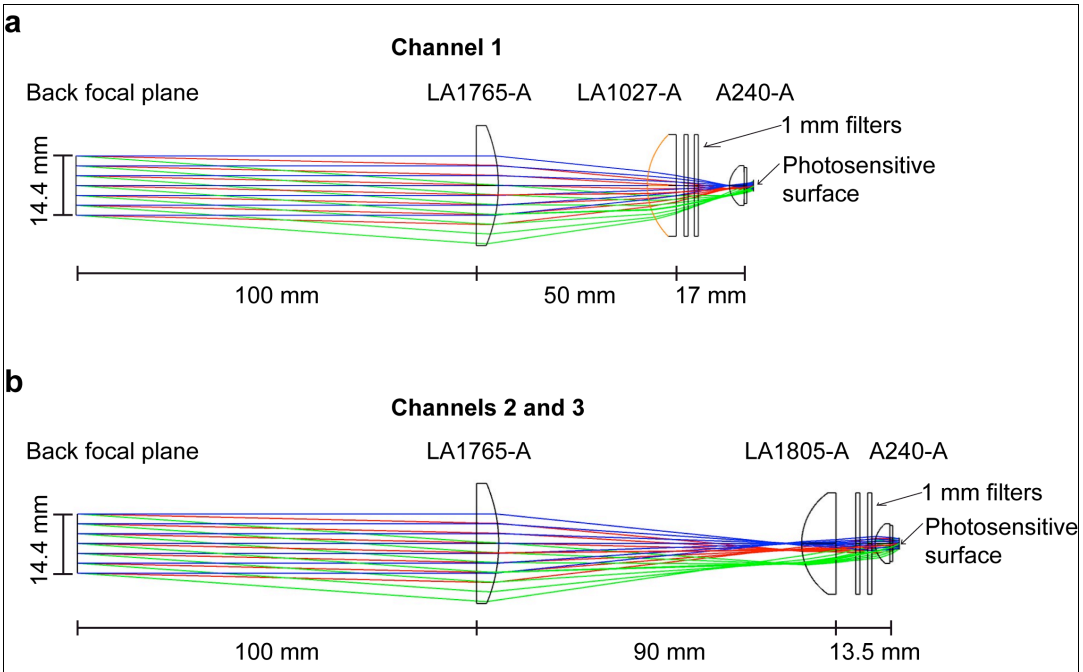

Supplementary Figure 3

Design of detection system using multi-pixel photon counting modules

Part numbers refer to lenses from Thorlabs.

(a) Short-arm channel.

(b) Long-arm channels.

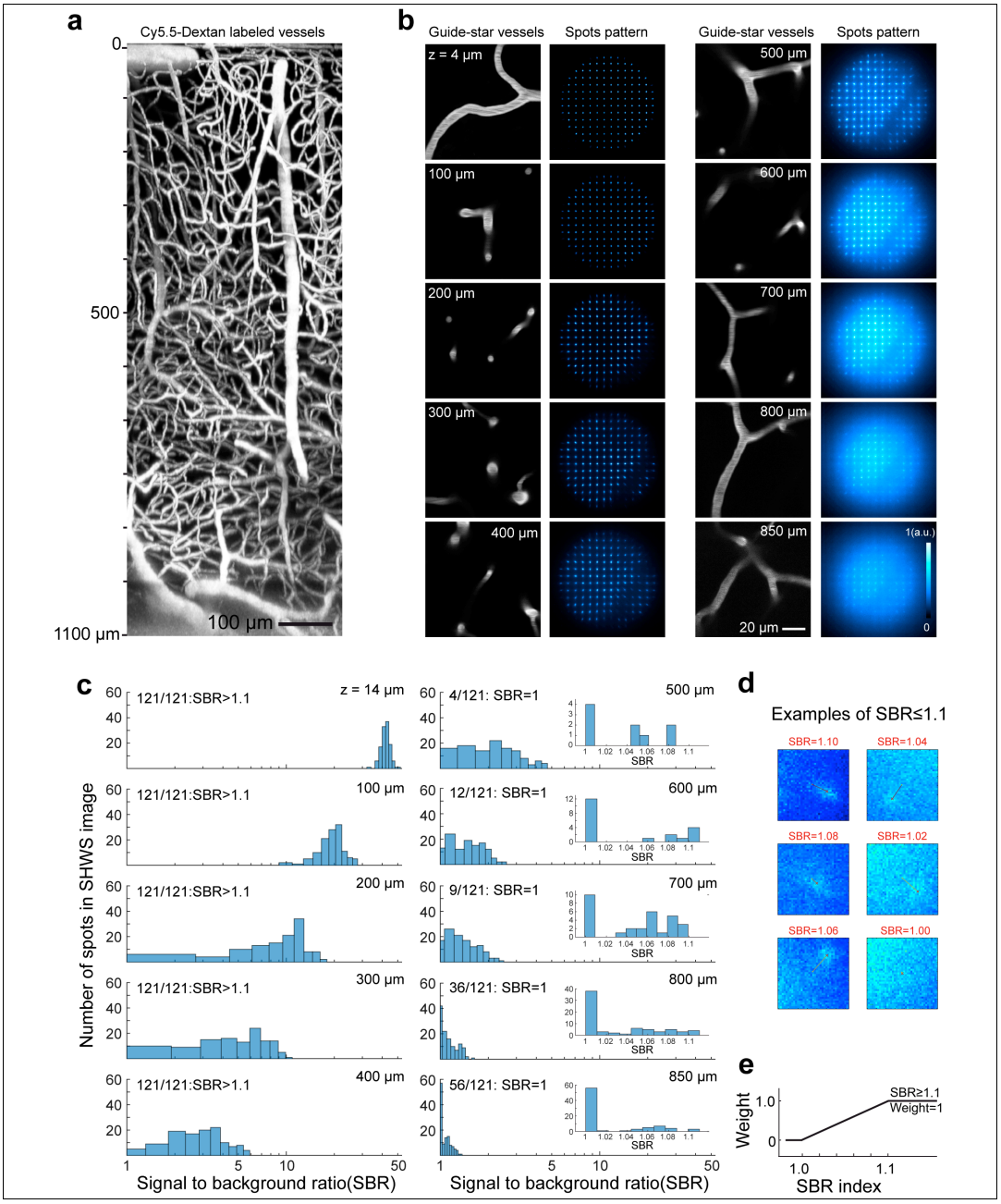
a
Cy5.5-Dextan labeled vessels
0
500
1100 μm
100 μm
b
Guide-star vessels
Spots pattern
Guide-star vessels
Spots pattern
z = 4 μm
100 μm
200 μm
300 μm
400 μm
500 μm
600 μm
700 μm
800 μm
850 μm
1(a.u.)
0
20 μm
c
121/121:SBR>1.1
z = 14 μm
4/121: SBR=1
500 μm
12/121: SBR=1
600 μm
9/121: SBR=1
700 μm
36/121: SBR=1
800 μm
56/121: SBR=1
850 μm
SBR
Number of spots in SHWS image
Signal to background ratio(SBR)
Signal to background ratio(SBR)
d
Examples of SBR≤1.1
SBR=1.10
SBR=1.04
SBR=1.08
SBR=1.02
SBR=1.06
SBR=1.00
e
Weight
SBR≥1.1
Weight=1
SBR index

Supplementary Figure 4
Wavefront sensing at depths up to 850 μm in living mouse cortex
The signal-to-background ratio (SBR) of the spots image acquired by Shack-Hartmann wavefront sensor decays as the depth increases as a result of tissue scattering. **(a)** Maximum intensity projections along x axis (Δx = 200 μm) of the cortical vasculature labeled by Cy5.5-dextran. **(b)** Guide-star microvascular images acquired by two-photon imaging at 14 μm to 850 μm below the pia and their corresponding spot images acquired by the SHWS during direct wavefront sensing. **(c)** Histograms of the SBR at different depths for the data on panel **b** with enlarged histograms of the SBR≤1.1 shown as subgraphs from 500-μm to 850-μm depth. **(d)** Examples of the wavefront image spots with the SBR below the value 1.1. **(e)** Weight distribution as a function of SBR that is used for wavefront reconstruction.

Microsoft Office User 4/23/2019 7:36 PM
Comment [3]: Vasculature?

Rui Liu 4/26/2019 4:24 PM
Comment [4R3]: agree

Rui Liu 4/26/2019 4:35 PM
Deleted: vascular

Microsoft Office User 4/23/2019 7:37 PM
Comment [5]: That is used?

Rui Liu 4/26/2019 4:28 PM
Comment [6R5]: agree

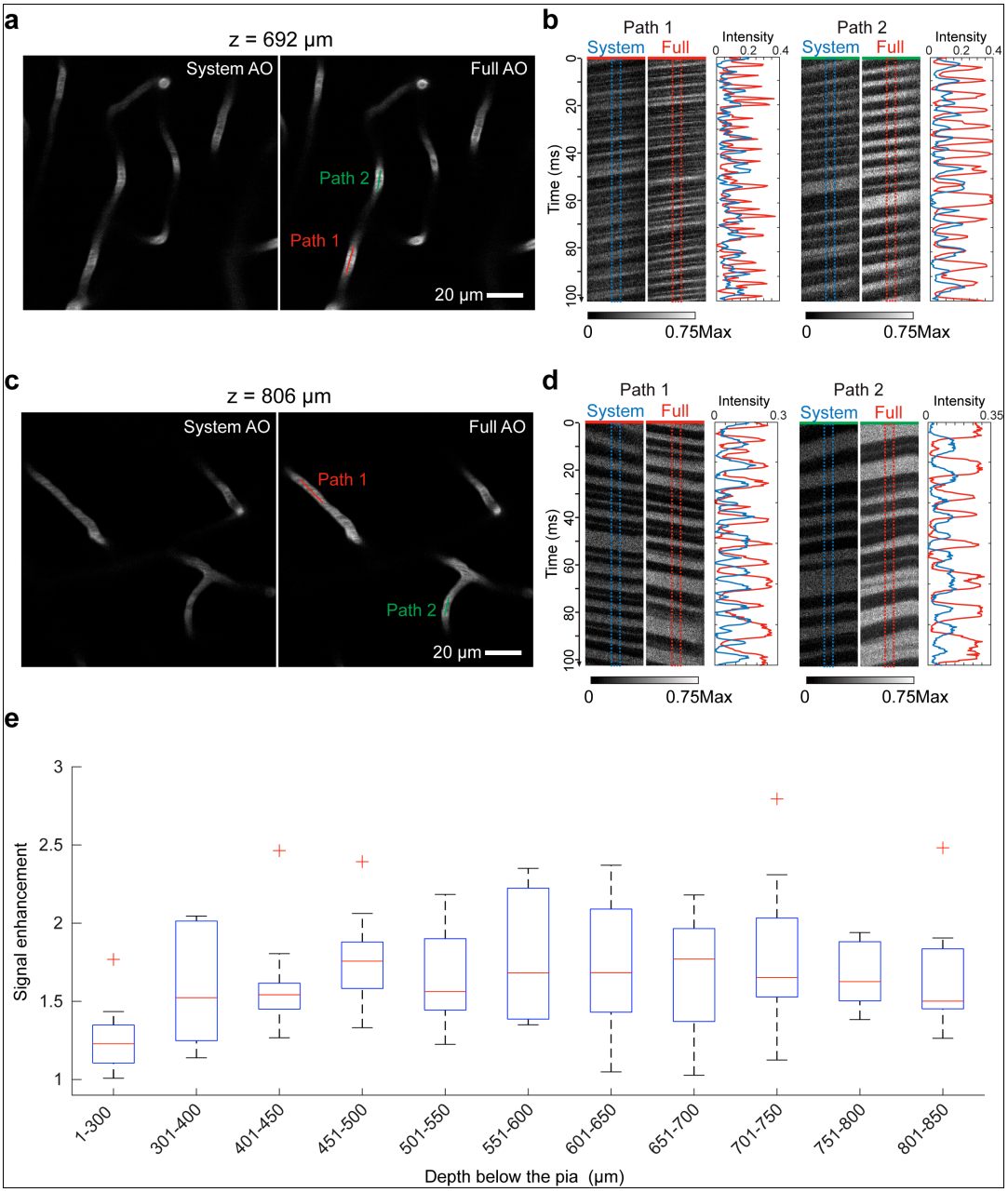
a
z = 692 μm
System AO
Full AO
Path 2
Path 1
20 μm
b
Path 1
System
Full
Intensity
Path 2
Time (ms)
0
0.75Max
c
z = 806 μm
d
e
Signal enhancement
Depth below the pia (μm)
1-300
301-400
401-450
451-500
501-550
551-600
601-650
651-700
701-750
751-800
801-850

Supplementary Figure 5

Full AO correction enhance the signal of Cy5.5-dextran labeled vascular and red blood cell flux in line scan at depth

(a) Imaging of vascular labeled by Cy5.5-dextran at 692 μm depth below the pia with System and Full AO correction.

(b) Red blood cell flux shown as line scan signals along the red and green lines in **a** are compared between System and Full AO.

(c,d) Same imaging as panels **a** and **b** but at a depth of 806 μm below the pia.

(e) Dependence of signal enhancement of red blood cell flux by AO correction as a function of the depth below the pia. Signal enhancement is defined as the ratio of peak-to-valley contrast of the line scan image of Full AO to System AO. 120 measurements over 3 mice were computed and shown in boxplot with maximum, minimum, third quartile, first quartile and median ($n \geq 6$).

Rui Liu 4/26/2019 5:56 PM
Comment [7]: We changed the order of supplementary figure 7 now to supplementary figure 5

Rui Liu 4/26/2019 5:53 PM
Deleted: 7

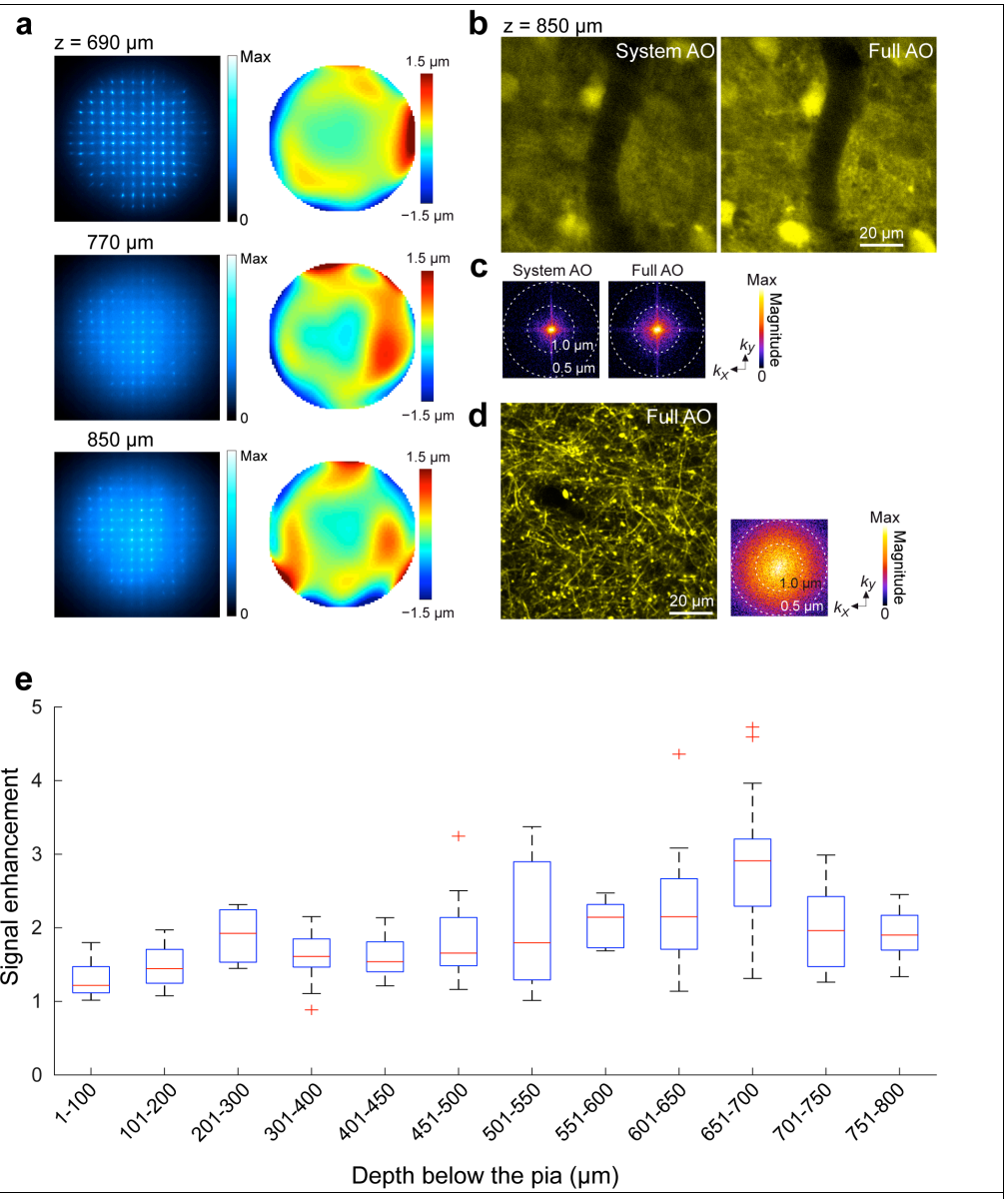

Supplementary Figure 6

Wavefront patterns, diffraction limited pia image used for k-space analysis in Figure 2 and signal

Rui Liu 4/26/2019 5:53 PM
Deleted: 5

Microsoft Office User 4/23/2019 7:37 PM
Comment [8]: Please check.

Rui Liu 4/26/2019 4:28 PM
Comment [9R8]: corrected

Rui Liu 4/26/2019 4:28 PM
Deleted: of

enhancement analysis
(a) Images of SHWS spots and corresponding wavefronts used for correction in panels **a**, b and e of Fig. 2, respectively.
(b,c) Images and corresponding spatial frequencies at 850-μm depth with System AO and Full AO correction used in panel e of Fig. 2.
(d) Diffraction limited image of apical dendrites and spines in pia that used in the *k*-space comparison in panel e of Fig. 2.
(e) Dependence of signal enhancement by AO correction as a function of the depth below the pia. Signal enhancement was calculated by the ratio of peak-to-valley contrast of the line profiles across the fine process in the neuronal images in vS1 between Full AO and System AO. About 190 measurements of dendrites and spines at different depth of vS1 cortex in 5 Thy1-YFP or Thy1-jRGECO1a mice were shown in the boxplot with maximum, minimum, third quartile, first quartile and median (n ≥ 5).

Rui Liu 4/26/2019 5:59 PM
Comment [10]: These changes adapt to the modification of figure 2

Rui Liu 4/26/2019 5:21 PM
Deleted: d

Rui Liu 4/26/2019 5:21 PM
Deleted: h

Rui Liu 4/26/2019 5:22 PM
Deleted: h

Rui Liu 4/26/2019 5:22 PM
Deleted: h

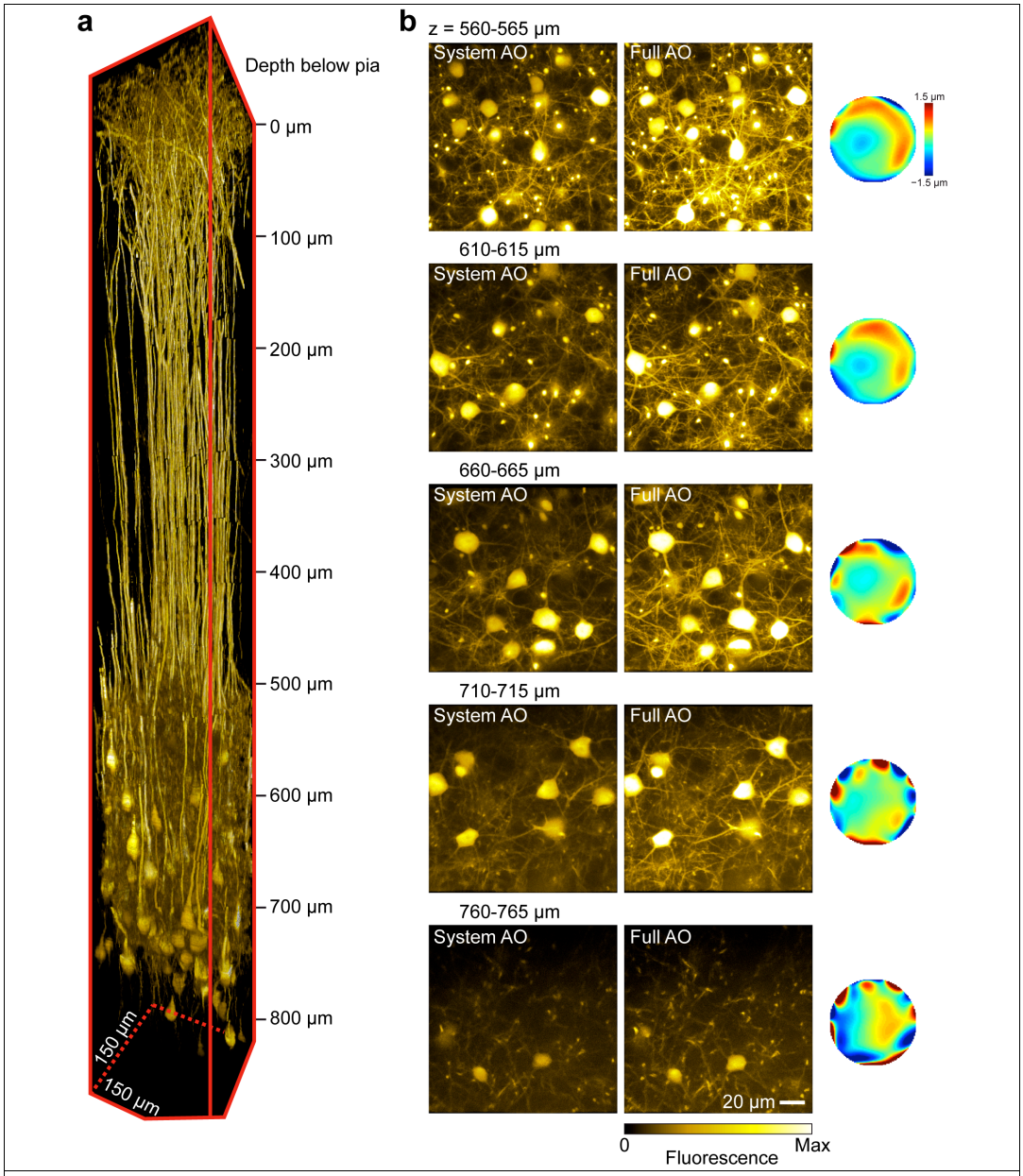

Supplementary Figure 7

Rui Liu 4/26/2019 5:53 PM
Deleted: 6

High-resolution imaging through layer 5b vS1 cortex in a Rbp4-cre mouse labeled by mRuby2
(a) The three dimensional image stack from *in vivo* imaging of mRuby2 labeled layer 5 pyramid neurons in a 150×150×810 μm^3 volume of vS1 cortex at an excitation wavelength of λ = 1.07 μm. Full AO corrections were measured and applied every 50 μm of depth. An enlarged view of Fig. 2. **(b)** Images at different depths, from 560 to 765 μm below the pia, with System AO and Full AO corrections. The corresponding correcting wavefront is shown.

Rui Liu 4/26/2019 5:23 PM
Deleted: i

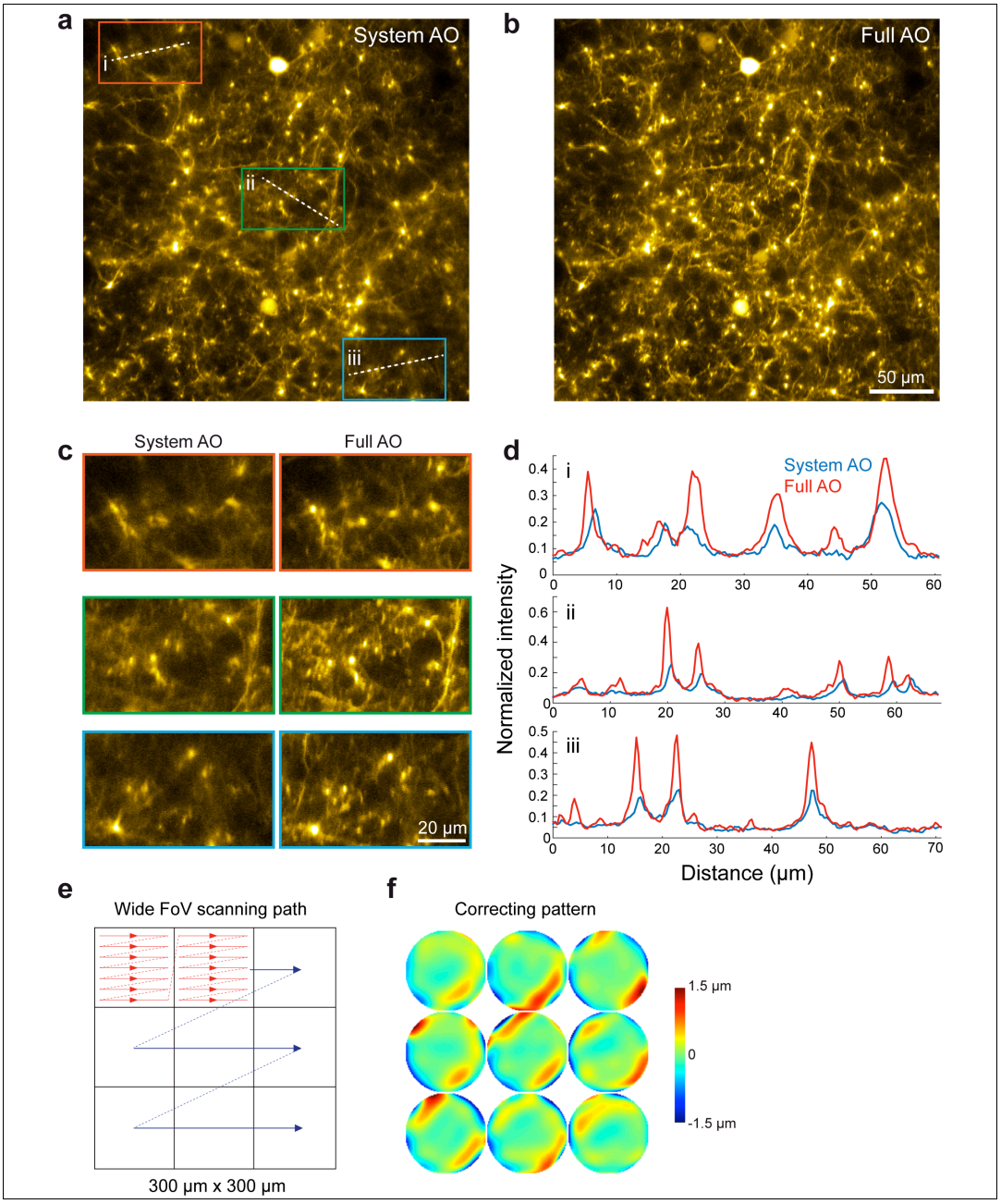
a
System AO
i
ii
iii
b
Full AO
50 μm
c
System AO
Full AO
20 μm
d
System AO
Full AO
i
ii
iii
Normalized intensity
Distance (μm)
e
Wide FoV scanning path
300 μm x 300 μm
f
Correcting pattern
1.5 μm
0
-1.5 μm

Supplementary Figure 8
Adaptive optics correction over wide field at a depth of 570 μm below pia
The subject is a Thy1-YFP mouse. **(a,b)** Images tiled by 3×3 sub-region scanning with System AO correction and Full AO correction are compared. **(c)** Zoom-in view of the boxes region of the image in **a** to compare the images with System and Full correction at different regions over a wide field. **(d)** Signal profiles of the white lines in **a** are compared between System and Full AO as a representative of 3 measurements in 2 mice. **(e)** Scanning path for wide field AO imaging with corresponding subregion wavefronts as shown in **f**, which were sequentially applied onto the DM and synchronized to sub-region switching by internal triggers. **(f)** Full AO correcting wavefronts used in panel **b**.

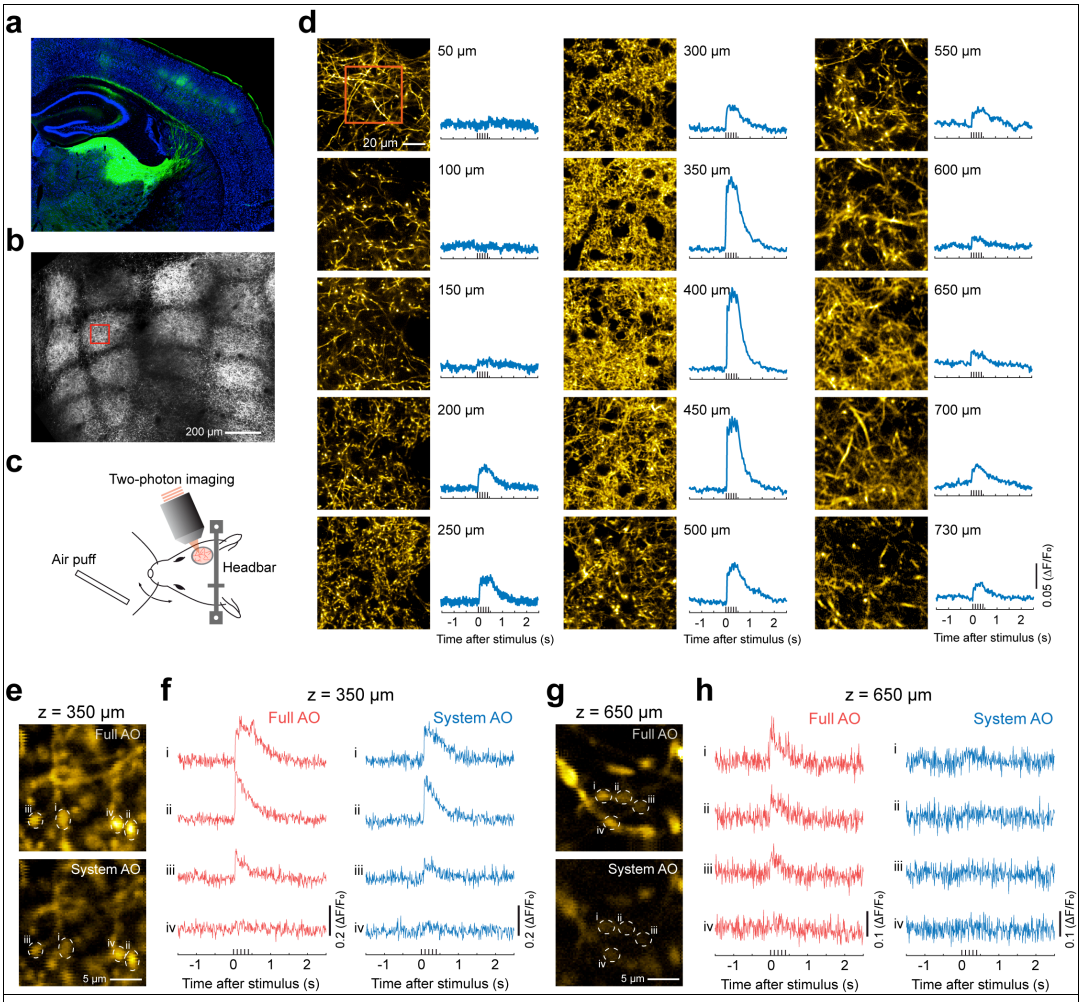

Supplementary Figure 9

In vivo imaging of glutamate response of thalamocortical axons in vS1 cortex during vibrissa stimulation with full AO

(a) Coronal section of the mouse brain shows the projection from VPM thalamus to vS1 cortex labeled by SF-Venus-iGluSnFR.A184S.

(b) *In vivo* two-photon imaging of the thalamocortical axons in layer 4 of vS1 cortex is shown as the

representative of 4 mice. Red box indicates the imaging region shown in panel **d**.

(c) Air puff whisker stimulation during two-photon imaging.

(d) Two-photon imaging of SF-Venus-iGluSnFR.A184S shows the glutamate release from thalamocortical axons and boutons varies as a function of depth as the representative of 7 measurements across 4 mice. Glutamate responses are averaged over the ROI defined by the red box region for all depths.

(e,f) Comparison between System AO and Full AO correction on functional imaging of thalamocortical axons and boutons that express SF-Venus-iGluSnFR.A184S at 350 μm below the pia. Corresponding glutamate responses to vibrissa stimulation in the ROIs defined by the dashed circles are shown in panel **f**.

(g,h) Same as panels **e** and **f** but at the depth of 650 μm. Experiments in panels **e**-**h** were repeated in 2 mice.

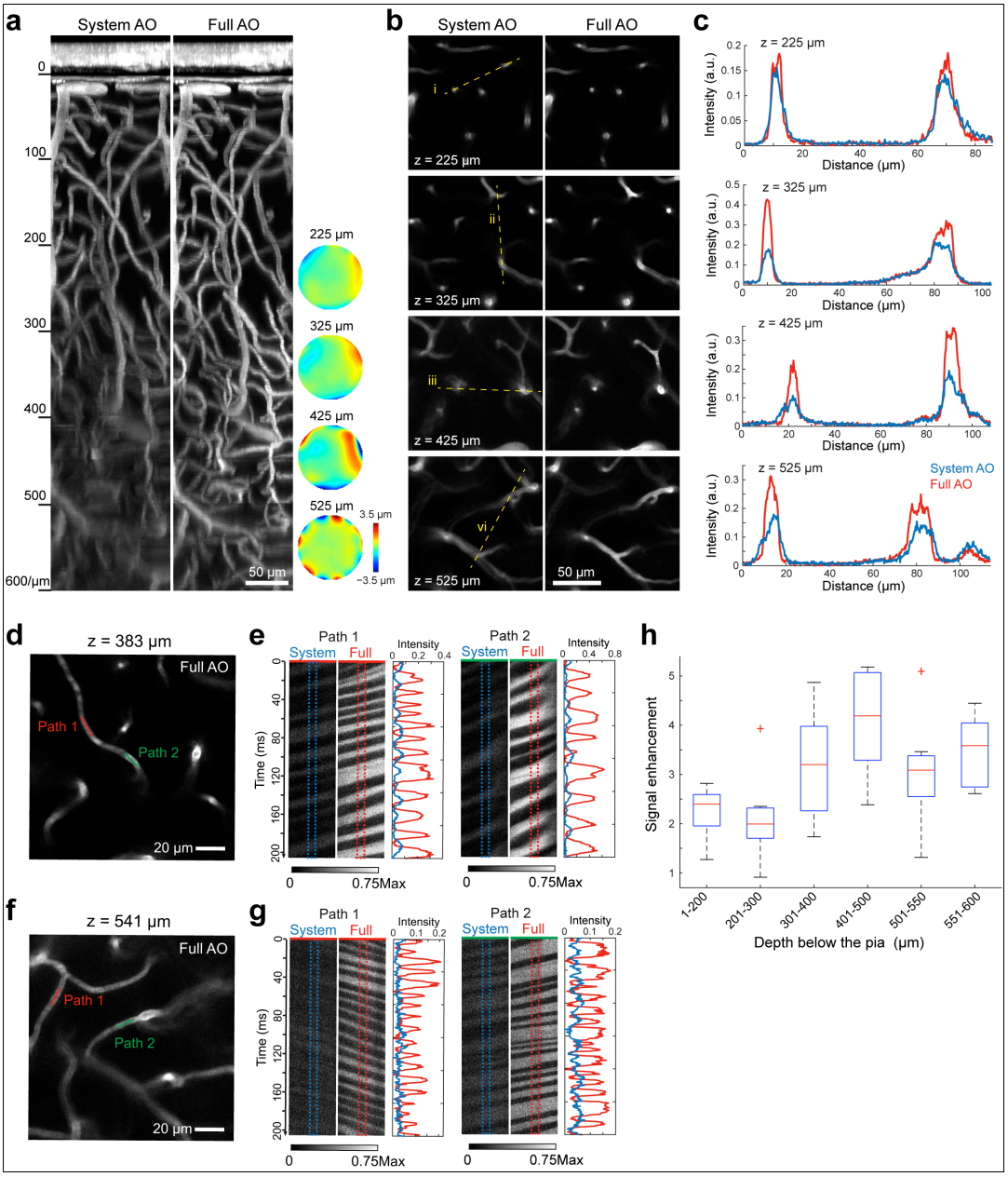
a
System AO
Full AO
0
100
200
300
400
500
600/μm
50 μm
225 μm
325 μm
425 μm
525 μm
3.5 μm
−3.5 μm
b
System AO
Full AO
i
ii
iii
vi
z = 225 μm
z = 325 μm
z = 425 μm
z = 525 μm
50 μm
c
z = 225 μm
z = 325 μm
z = 425 μm
z = 525 μm
Intensity (a.u.)
Distance (μm)
System AO
Full AO
d
z = 383 μm
Full AO
Path 1
Path 2
20 μm
e
Path 1
Path 2
System
Full
Intensity
Time (ms)
0
0.75Max
f
z = 541 μm
Full AO
Path 1
Path 2
20 μm
g
Path 1
Path 2
System
Full
Intensity
Time (ms)
0
0.75Max
h
Signal enhancement
1-200
201-300
301-400
401-500
501-550
551-600
Depth below the pia (μm)

Supplementary Figure 10

Full AO correction enables imaging of Cy5.5-dextran labeled vascular and red blood cell flux through the polished and reinforced thinned-skull window at depth in vS1 cortex

(a) Maximum intensity projections on y axis of the 140 × 140 × 600 μm^3 volume images are compared between System (left) and Full (right) AO correction. Wavefronts at four different depths are shown on the right. Experiments were repeated in 2 mice with 2 measurements across depths.

(b) Lateral images at 225, 325, 425 and 525 μm depth belong to the volume shown in panel **a** are compared between System (left) and Full AO (right) correction.

(c) Signal profiles along the yellow dashed line in panel **b** are compared between System (blue) and Full AO (red) correction.

(d) Imaging of vascular labeled by Cy5.5-dextran at 383 μm depth through the thinned-skull window with Full AO correction.

(e) Red blood cell flux shown as line scan signals along the red and green lines in panel **d** are compared between System and Full AO.

(f,g) Same imaging as panels **d** and **e** but at a depth of 541 μm below the pia.

(h) Dependence of signal enhancement of red blood cell flux by AO correction as a function of the depth below the pia. Signal enhancement is defined as the ratio of peak-to-valley contrast of the line scan image of Full AO to System AO. 60 measurements over 3 mice were computed and shown in the boxplot with maximum, minimum, third quartile, first quartile and median ($n \geq 6$).

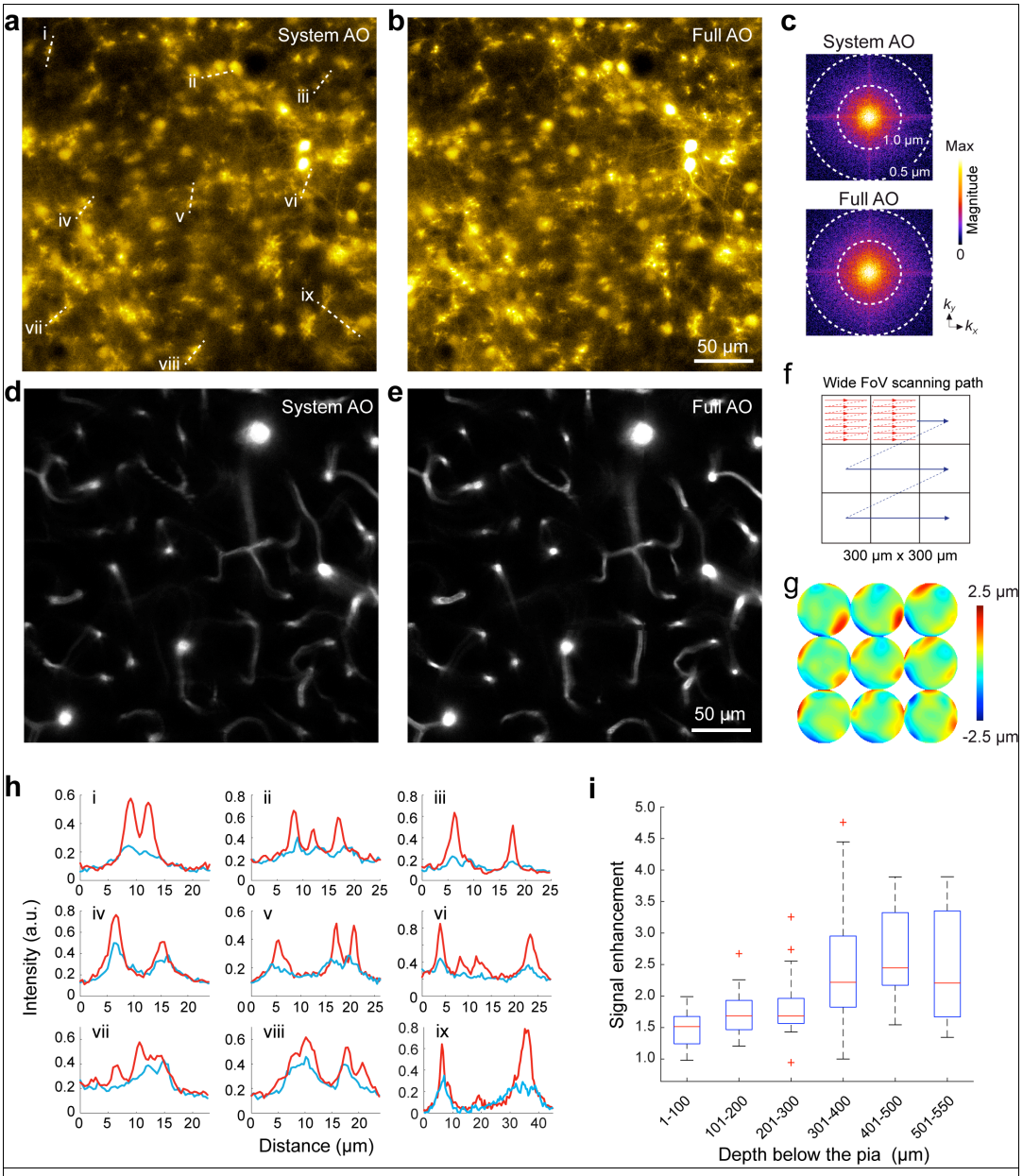

Supplementary Figure 11

Wide-field imaging through thinned-skull window with Full AO and signal enhancement analysis
(a,b) Neuronal images at 320 μm below the pia in S1 cortex of Thy1-YFP mouse with System AO and Full AO correction and corresponding ***k***-space map shown in panel **c**. **(d,e)** Vascular images at the same region of panel **a** with System AO and Full AO corrections. **(f)** Tiled scanning path is used for wide field AO imaging, same as in Supplementary Fig. 8. **(g)** Wavefronts used for correction in panels **b** and **e**. **(h)** Signal profiles along the dashed lines in panels **a** and **b** respectively, are compared between System AO (blue trace) and Full AO (red trace) correction. **(i)** Signal enhancement was calculated by the ratio of peak-to-valley contrast of the line signal profiles across the fine process in the neuronal images in vS1 between Full AO and System AO. 128 measurements in 3 Thy1-YFP or Thy1-jRGECO1a mice were shown as the boxplot with maximum, minimum, third quartile, first quartile and median (n ≥ 10).

Microsoft Office User 4/23/2019 7:42 PM
Comment [11]: "enhancements were" or "enhancement was"?

Rui Liu 4/26/2019 4:31 PM
Comment [12R11]: corrected

Rui Liu 4/26/2019 4:31 PM
Deleted: were

Rui Liu 4/26/2019 4:31 PM
Deleted:

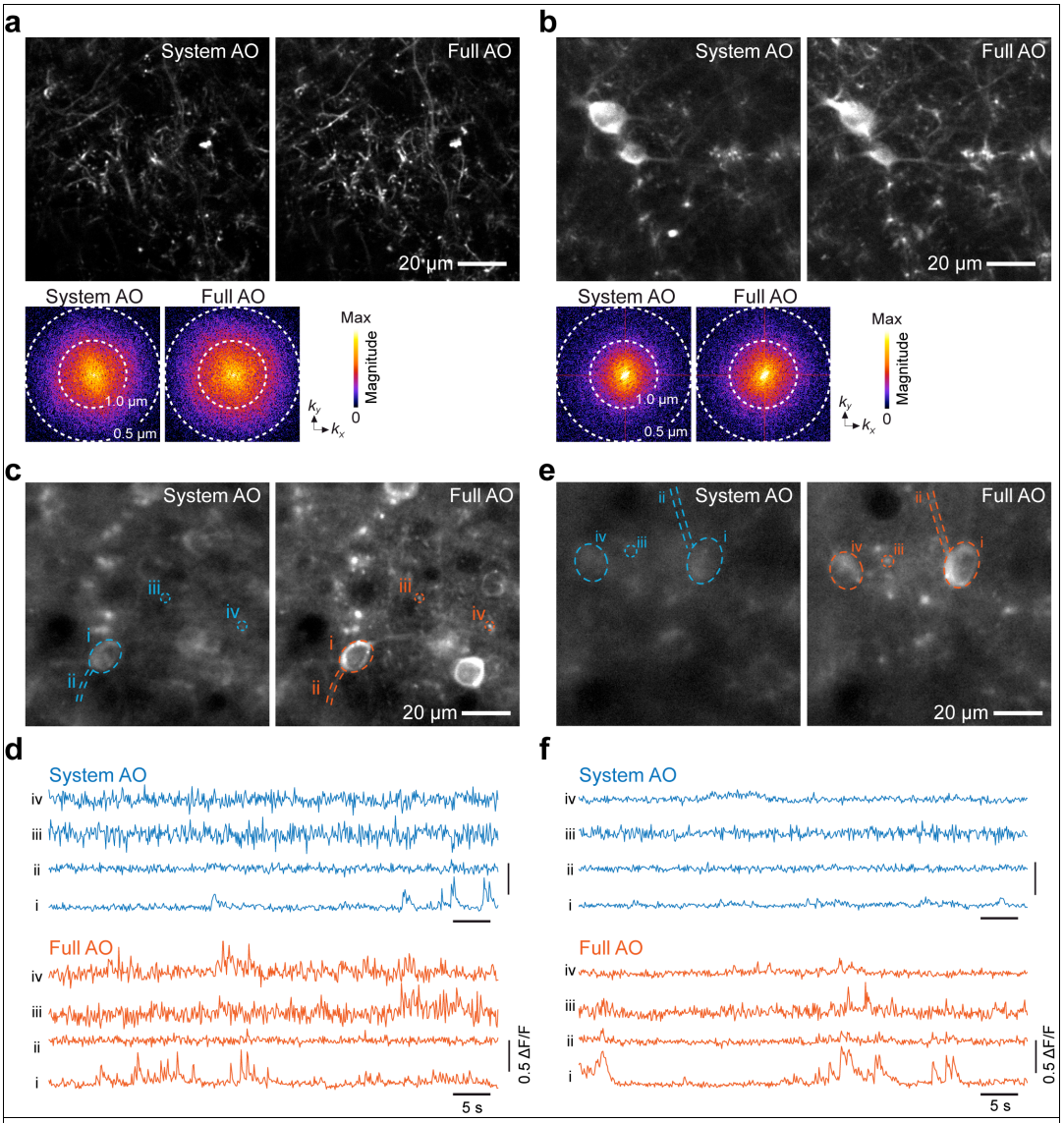

Supplementary Figure 12

Adaptive optics correction enables neuronal morphological and functional imaging through a thinned-skull window down to 500 μm below the pia

(a,b) Imaging of apical dendrites and spines labeled by jRGECO1a at the depth of 100 μm and 220 μm below the pia through the thinned skull window with adaptive optics.

(c) Functional imaging of barrel cortex at 386 μm below pia in Thy1-jRGECO1a mouse with System and Full AO correction are shown.

(d) Spontaneous calcium transients within the ROIs in compared between System AO (blue trace) and Full AO (red trace) corrections.

(e,f) Same imaging as panels **a** and **b** but at a depth of 520 μm below the pia. Note that for ROI calcium transient calculation, neuropil responses are subtracted by using the surround regions. 3 measurements at similar depth as panels **e** and **f** were repeated.

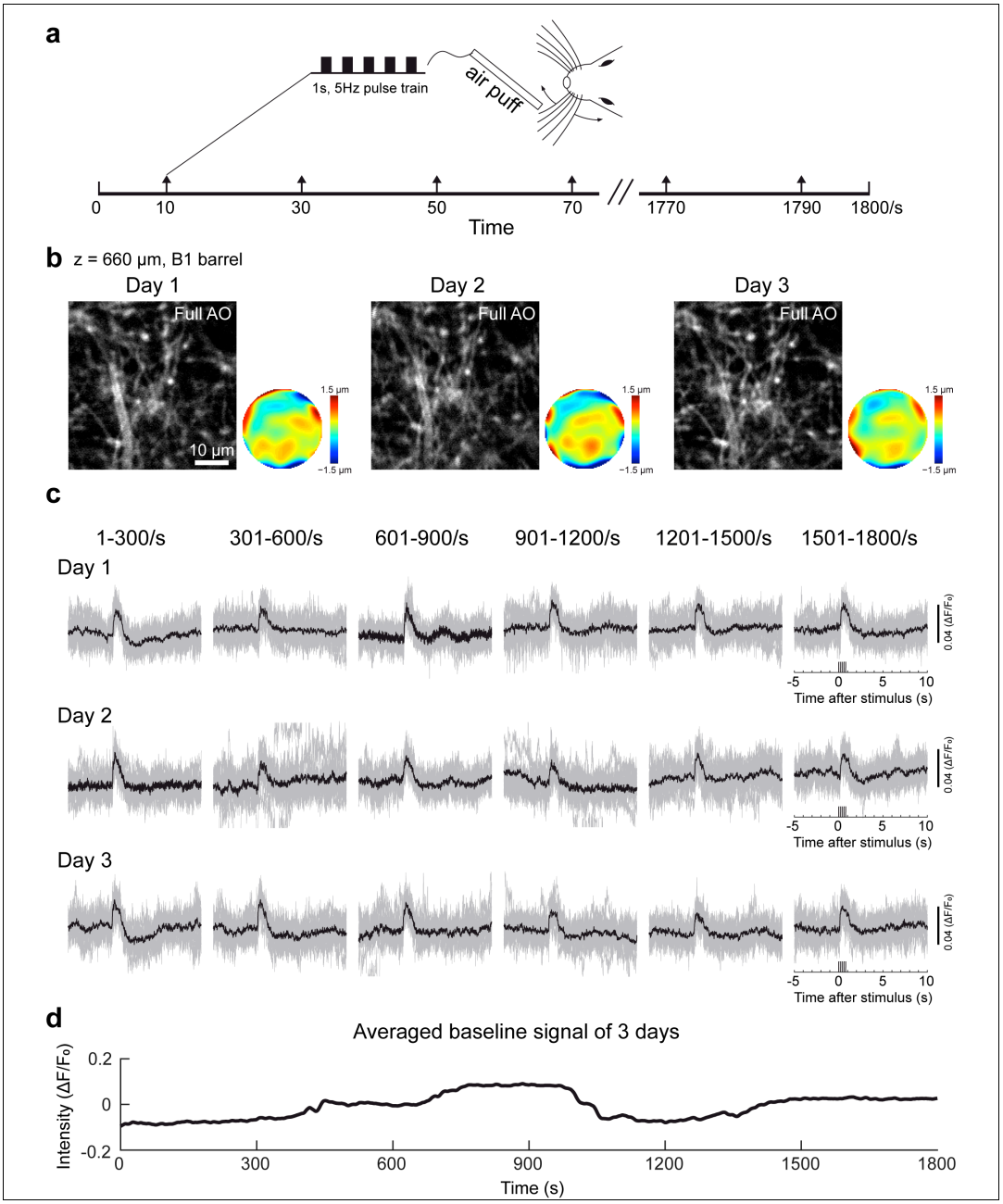
a
1s, 5Hz pulse train
air puff
0
10
30
50
70
1770
1790
1800/s
Time
b
z = 660 µm, B1 barrel
Day 1
Day 2
Day 3
Full AO
10 µm
1.5 µm
−1.5 µm
c
1-300/s
301-600/s
601-900/s
901-1200/s
1201-1500/s
1501-1800/s
Day 1
Day 2
Day 3
0.04 (ΔF/F₀)
-5
0
5
10
Time after stimulus (s)
d
Averaged baseline signal of 3 days
Intensity (ΔF/F₀)
0.2
0
-0.2
0
300
600
900
1200
1500
1800
Time (s)

Supplementary Figure 13
Assessing phototoxicity by measuring sensory evoked glutamate response of thalamocortical axons in vS1 L5 during chronic imaging with adaptive optics
(a) Experiment of 30-minutes continuous imaging with rhythmic air puff whisker stimulation. **(b)** The experiment as in panel **a** were repeated at same location for 3 days. Images of the thalamocortical axons labeled by SF-Venus-iGluSnFR.A184S at the same region of B1 barrel at the depth of 660 µm and corresponding wavefronts for each day are shown. **(c)** Sensory evoked glutamate signals of the axons in the imaging field were averaged every 5 minutes (n = 15 trials) and shown during 30-minutes continuous imaging for each day. **(d)** Averaged glutamate baseline signal of 3 days based on 3 measurements.

Microsoft Office User 4/23/2019 7:43 PM
Deleted: ally

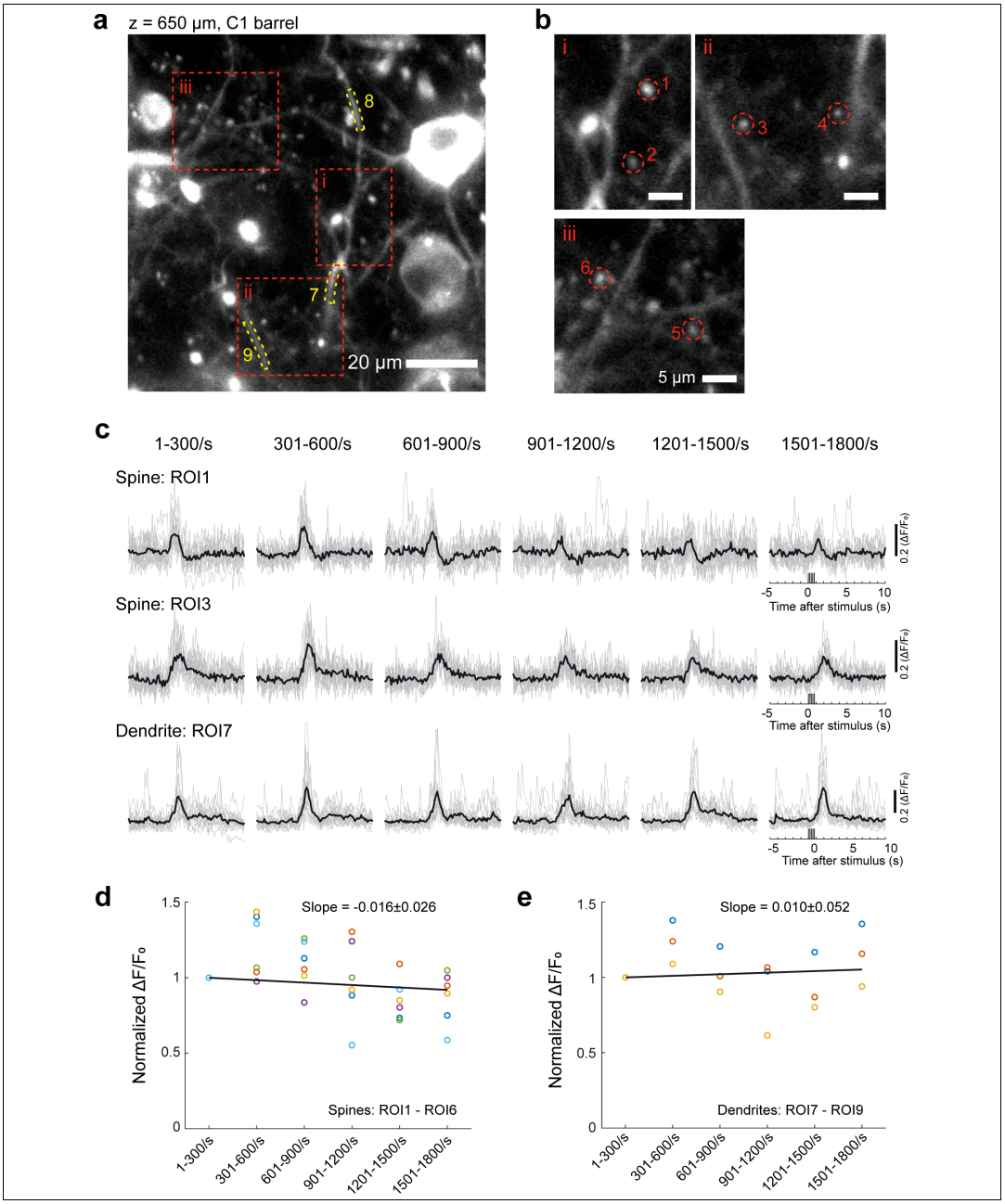
a
z = 650 µm, C1 barrel
iii
8
i
ii
7
9
20 µm
b
i
1
2
ii
3
4
iii
6
5
5 µm
c
1-300/s
301-600/s
601-900/s
901-1200/s
1201-1500/s
1501-1800/s
Spine: ROI1
Spine: ROI3
Dendrite: ROI7
0.2 (ΔF/F₀)
-5 0 5 10
Time after stimulus (s)
d
Slope = -0.016±0.026
Normalized ΔF/F₀
1.5
1
0.5
0
Spines: ROI1 - ROI6
1-300/s
301-600/s
601-900/s
901-1200/s
1201-1500/s
1501-1800/s
e
Slope = 0.010±0.052
Normalized ΔF/F₀
Dendrites: ROI7 - ROI9

Supplementary Figure 14
Assessing phototoxicity by measuring sensory evoked calcium response of basal dendrites and spines in vS1 L5 during long-term imaging with adaptive optics
(a,b) Same experiment as in Supplementary Fig. 13a was performed. Images of the dendrites and spines labeled by jRGECO1a in C1 barrel region at 650-μm depth. **(c)** Sensory evoked calcium signals of the dendrites in ROI7 and spines in ROI1 and ROI3 shown in **a** and **b** were averaged every 5 minutes during 30-minutes imaging session (15 trials). **(d,e)** Normalized amplitudes of sensory evoked calcium signals of 6 spines in ROI1-ROI6 as in panel **b** and 3 dendrites in ROI7-ROI9 as in panel **a**. Slopes were calculated by linear regression fit with initial point constraints for each ROI datasets. The standard deviation and the mean of the slope values were calculated and shown in panel **d** (n = 6) and panel **e** (n = 3). The black lines indicates the fitting curve using mean slope with constraint initial point.

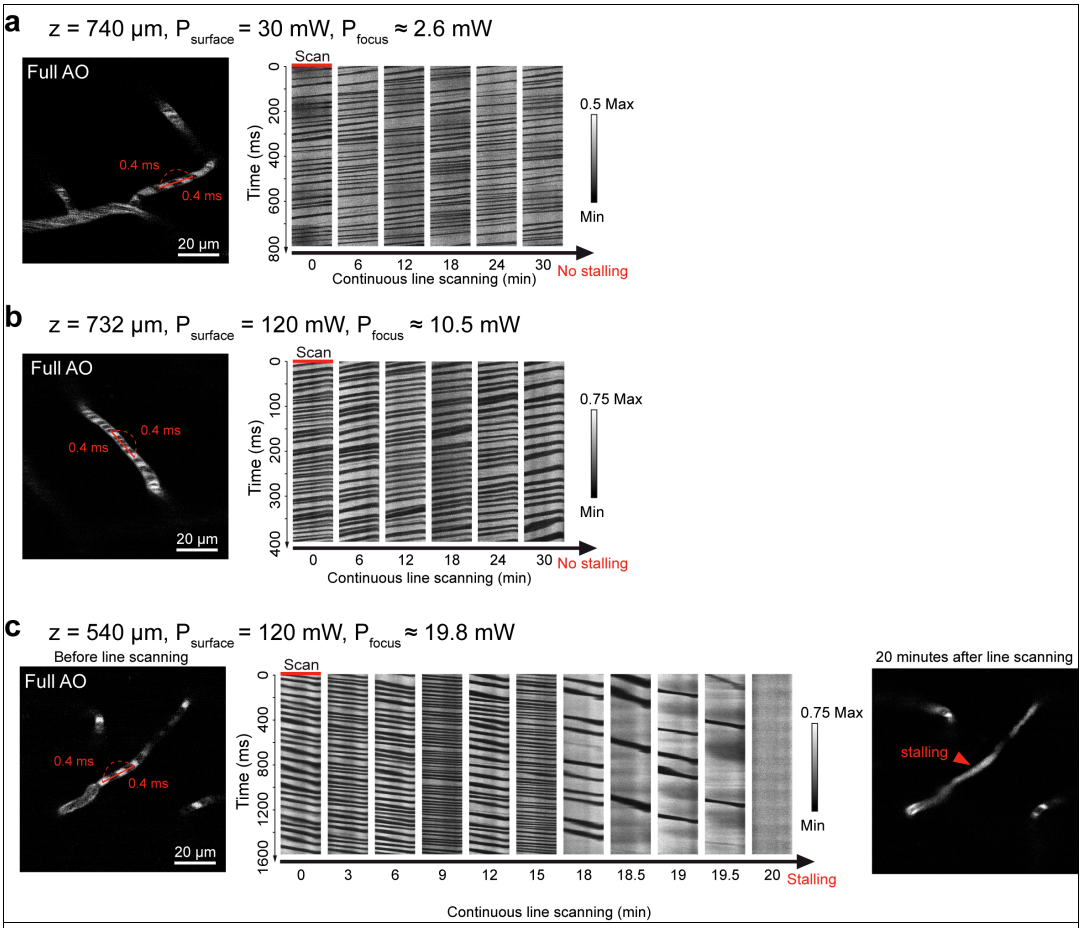

Supplementary Figure 15

Assessing phototoxicity by measuring red blood cell flux during long-term line scanning on capillary with adaptive optics

(a) Imaging of the capillary and line scanning along the path shown as red. 30-minutes continuous line scanning was performed at 740-μm depth below the pia. 800-ms red blood cell flux images at the beginning of each 5 minutes were shown during 30 minutes. Imaging power was adjusted minimum that allows to achieve sufficient single to noise for flux measurement. No stalling was observed.

(b) Line scanning imaging as **a** was performed on a capillary at the depth of 732 μm but with

maximum power. 400-ms red blood cell flux images at the beginning of each 5 minutes were shown during 30 minutes. No stalling was observed.

(c) Line scanning imaging as **a** was performed on a capillary at the depth of 540 μm with maximum power as in **b**. 1600-ms red blood cell flux images at the beginning of each 5 minutes were shown during 20 minutes. Stalling was observed after 20-minutes line scanning. Experiments at similar depth below the pia as panels **a**-**c** were repeated in 2 mice.